J Mater Sci (2015) 50:4980–4993
DOI 10.1007/s10853-015-9046-5

Evidence for magneto-electric and spin–lattice coupling in $PbFe_{0.5}Nb_{0.5}O_3$ through structural and magneto-electric studies

Shidaling Matteppanavar[1] · Sudhindra Rayaprol[2] · Kiran Singh[3] · V. Raghavendra Reddy[3] · Basavaraj Angadi[1]

Received: 8 October 2014 / Accepted: 21 April 2015 / Published online: 28 April 2015

Abstract Neutron diffraction (ND) studies were carried out on polycrystalline single-phase multiferroic $Pb(Fe_{0.5}Nb_{0.5})O_3$ (PFN) in the temperature range of 290–2 K to understand the structural and magnetic properties as a function of temperature. ND data were refined using the Rietveld refinement method for both crystallographic and magnetic structures. The structure at room temperature was found to be monoclinic, in *Cm* space group. No structural transition was observed till 2 K. At low temperatures (i.e., from $T < T_N$; $T_N = 155$ K), an additional peak appears at scattering vector, $Q = 1.35$ Å^{-1}, indicating the onset of antiferromagnetic ordering. The magnetic structure was found to be commensurate with the crystallographic structure and could be refined using the propagation vector, $k = [0.125, 0.5, \text{and } 0.5]$. Magnetization, ferroelectric P–E loops, and dielectric measurements on PFN reveal a strong anomaly at the antiferromagnetic transition temperature (T_N) indicating the magneto-electric coupling. The refined temperature-dependent structural parameters such as unit cell volume and monoclinic distortion angle (β) reveal pronounced anomalies at the magnetic ordering temperature (T_N), which indicates strong spin–lattice coupling. An anomaly in lattice volume was observed with a small negative thermal expansion below and a large thermal expansion above the T_N, respectively. It shows the occurrence of isostructural phase transition accompanying the magnetic ordering below $T_N \sim 155$ K, leading to significant change in ionic polarization, octahedral tilt angle, and lattice strain around T_N. We have used refined atomic positional coordinates from the nuclear and magnetic structures, to obtain ionic polarization. These detailed studies confirm the magneto-electric and spin–lattice coupling in PFN across T_N.

Introduction

In recent years, single-phase multiferroic materials have attracted much attention as they provide means to explore and understand details about the coexistence of magnetic and electric ordering [1]. The search for these materials is driven by the prospect of controlling charges by applying magnetic field and controlling spins by applying electric field. Such inter-controllability helps in developing new forms of multifunctional devices [1]. Among the single-phase lead-based multiferroic materials, $Pb(Fe_{0.5}Nb_{0.5})O_3$ (PFN) exhibits high dielectric constant and diffuse ferroelectric phase transition. PFN is an attractive candidate for the potential applications, such as multilayer ceramic capacitors and other electronic devices [2]. PFN exhibits ferroelectric phase transition (Curie temperature, T_C) at $\sim$380 K and antiferromagnetic ordering below its Néel temperature ($T_N \sim 143$ K) [2].

Although multiferroic properties have been well characterized both in single crystal [3–5] and ceramic form [6–8], there exists controversy about the structure of PFN. In a study using synchrotron X-ray diffraction for powder and single crystals of PFN, Bonny et al. [5] have reported a monoclinic ferroelectric structure at 293 K, which undergoes a structural transition at 355 K (for single crystals) to

✉ Basavaraj Angadi
brangadi@gmail.com

[1] Department of Physics, Bangalore University, Jnanabharathi Campus, Bangalore 560056, India

[2] UGC-DAE-Consortium for Scientific Research, Mumbai Centre, BARC Campus, Mumbai 400085, India

[3] UGC-DAE Consortium for Scientific Research, University Campus, Khandwa Road, Indore 452001, India

another ferroelectric phase with tetragonal symmetry. At 376 K, a phase transition to a paraelectric phase with cubic symmetry takes place. Some reports show PFN with rhombohedral structure (space group *R3m*) at room temperature, which undergoes a diffuse phase transition at 387 K to cubic *Pm3m* symmetry [9]. A recent work on single crystals has suggested a small monoclinic distortion away from rhombohedral symmetry at room temperatures, along with the existence of an intermediate phase of tetragonal symmetry at temperatures between 355 K and the ferroelectric Curie point of 376 K [5]. Moreover, antiferromagnetic G-type spin ordering has been found in powder PFN samples at temperatures below $T_N = 143$ K [2, 10]. However, the T_N values for PFN have been reported to be widely scattered from lowest value of 143 K [10] to the highest value of 200 K [11]. The large scattering of T_N (143–200 K) in PFN is mainly due to the fluctuations in the local ordering of Nb and Fe ions [11] and/or to local clustering of Fe ions. It may also be due to the varied synthesis methods adopted, which leads to grain growth with lattice strain/stress in the material and these parameters affects the T_N.

These results of structural complexity are consistent with the study of Lampis et al. [12] who performed neutron and X-ray diffraction experiments in PFN powders obtained by grinding single crystals, although the authors have shown a monoclinic distortion ("pseudo-rhombohedral" structure) in the ferroelectric phase i.e., at 80, 250, and 363 K. On the other hand, it has been pointed out that the structure of PFN ceramic samples corresponds to a rhombohedral symmetry [13]. In agreement with these results, Ivanov et al., refined the structure from neutron diffraction measurements in rhombohedral symmetry at 10 and 300 K [14]. However, more recently, it has been reported that PFN exhibits monoclinic structure with *Cm* space group from 12 K up to room temperature [2]. However, the nature of magnetic and nuclear structures is still not clearly understood, as Ivanov et al. [14] discussed the structure only at 10 and 300 K, while Singh et al. [2] reported only nuclear structure using synchrotron powder XRD. The disagreements in the earlier reports are the propelling reasons for present study.

In the light of above considerations, further investigation is required to confirm the existence of structural symmetry in this synthesis conditions and method. We have applied neutron diffraction technique in order to resolve the structural complexity of PFN. Neutron diffraction experiments measured at different temperatures from 290 to 2 K for better understanding of the nuclear and magnetic structures of the controversial PFN along with dielectric and magnetic properties. Detailed understanding of the structural properties is very important because all magnetic and ferro-dielectric properties are structural dependent. From the analysis of the structural refinements, it is shown that the lattice parameters and unit cell volume show distinct anomaly at T_N, with unambiguous evidence of small negative thermal expansion and a large thermal expansion below and above the T_N, respectively. These structural anomalies are well reflected in magnetic, ferro-dielectric properties which indicates the presence of strong correlation between the structural properties and magnetic, ferro-dielectric properties and this is the direct evidence of spin–lattice coupling.

Experimental

Sample preparation and characterization

The single-phase PFN samples were synthesized using the single-step solid-state reaction method using the stoichiometric quantities of $Pb(NO_3)_2$, Fe_2O_3, and Nb_2O_5 (analytical grade) powders [15, 16]. The powders of all the starting materials were mixed thoroughly using agate pestle and mortar in an ethanol medium for 2 h. The mixture was then calcined at 973 K for 2 h. The calcined mixture was reground and cold pelletized into 5 mm diameter and 2–3-mm thick pellets, and then sintered at 1323 K for 1 h in a specially designed Pb-rich environment. The Pb-rich environment was created inside a sealed crucible containing Pb source with equal proportion of PbO and ZrO_2 to minimize the Pb evaporation. The samples were characterized with the powder X-ray diffraction using Phillips (1070 model) diffractometer with CuK_α radiation ($\lambda = 1.5406$ Å) for the phase formation. The data were recorded between 10° and 70° (2θ scans) in steps of 0.02°.

Magnetization studies were carried out on a vibrating sample magnetometer (VSM) attached to a physical property measurement system (*Quantum Design* PPMS). The dc magnetic susceptibility data were collected in the temperature range 5 K $< T <$ 400 K with an applied magnetic field of 500 Oe.

For the electrical characterization, the samples were thinned to make parallel plate capacitor geometry, and electrodes were made using Ag paint and fired at 100 °C for 5 min. The temperature-dependent dielectric permittivity was measured using an Agilent E4980A LCR meter with a home-made sample holder integrated with the commercial Physical Properties Measurement System (PPMS, Quantum Design).

The ferroelectric (*P–E*) loop measurements were carried out at different temperatures (100, 130, 150, 200, 250, and 300 K) by ferroelectric loop (*P–E*) tracer (M/s Radiant Instruments, USA). Thin silver paste is applied on both sides (top and bottom) of the PFN pellet as the electrodes. For room temperature *P–E* measurements, the samples

were immersed in silicone oil to prevent the electric arcing, if any, at high applied voltages.

Neutron diffraction and refinement

The neutron diffraction (ND) experiments were carried out using a position-sensitive detector based focusing crystal diffractometer installed by the UGC-DAE CSR Mumbai Centre at Dhruva reactor, Trombay India. The sintered pellets of 5 mm diameter kept inside a vanadium can were used for the experiment. The diffraction data were collected using a wavelength of 1.48 Å in the temperature range of 290–2 K and in the 2θ range of 6°–120°. ND data were refined by Rietveld refinement method using the *Fullprof* suite programs.

Results and discussion

XRD at room temperature

Achieving a single-phase PFN has been a challenge for the researchers due to the formation of detrimental secondary phases, such as pyrochlores, along with the perovskite phase. One of the reasons for the formation of pyrochlore phases is the evaporation of Pb above 850 °C during the sintering process. In order to avoid the formation of pyrochlore phase, Pb evaporation has to be controlled. To achieve this, we have used a Pb-rich closed environment during the sintering process. $PbZrO_3$ was used as a Pb source inside the closed environment, which is sealed to control the Pb partial pressure. Figure 1a shows the Rietveld refined powder XRD pattern of sintered PFN at room temperature. All the peaks of the XRD pattern could be indexed to the PFN monoclinic perovskite structure with *Cm* space group. The synthesis method described above has resulted in achieving the single-phase PFN [16]. The inset of Fig. 1a depicts the zoomed profiles of the pseudocubic (2 0 0), (2 2 0) and (2 2 2) reflections which show the monoclinic splitting. The (2 0 0) reflection show the clear evidence of doublet feature with the appearance of a shoulder and it is the direct evidence for the monoclinic structure with *Cm* space group. Refinement carried out with the monoclinic structure and *Cm* space group shows good fitting with low *R* factors and χ^2. The efforts of refinement considering rhombohedral structure with *R3m* space group, resulted in very high *R* factors and χ^2.

Room temperature structure using ND

As a starting model, the 290 K ND data were refined for the nuclear structure with the *monoclinic* symmetry (space group *Cm*). We have considered it as our starting model as

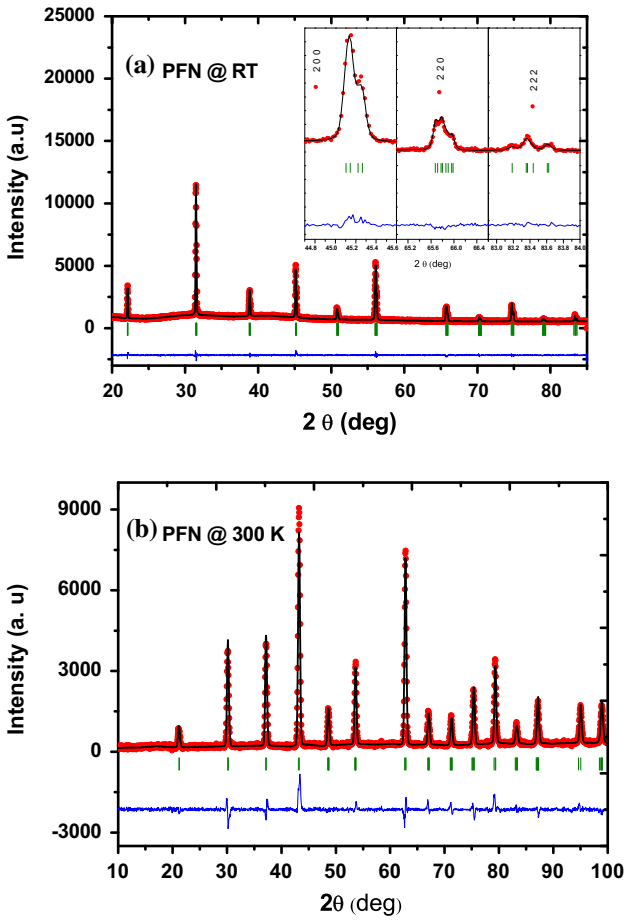

Fig. 1 Rietveld refined **a** X-ray diffraction and **b** Neutron diffraction data of $PbFe_{0.5}Nb_{0.5}O_3$ with *Cm* space group at room temperature

the controversy over structure in PFN, due to the various reported models, was narrowed down to the monoclinic symmetry [2]. During the refinements, the atoms were first fixed at their special positions in the *monoclinic* (*Cm*) symmetry. Figure 1b shows the Rietveld refined data (at 290 K) with the evident reasonable fitting between the experimental and the calculated patterns. The cationic and oxygen content was observed to be as per the expected composition of $Pb(Fe_{0.5}Nb_{0.5})O_3$. The atomic ratio between the Fe and Nb was close to unity and the total oxygen content remained to be 3, confirming the formation of stoichiometric single phase of the studied material. The obtained lattice parameters; $a = 5.6802$ (5) Å, $b = 5.6723$ (4) Å, $c = 4.0273$ (4) Å, and $\beta = 89.820°(8)$ are in excellent agreement with reported results [2]. The refined structural parameters obtained after the Rietveld refinement of ND data at 290 K are shown in Table 1.

For refinements, considering Pb with isotropic (U_{iso}) thermal parameters found to be invariably high. Hence, the refinements were done with anisotropic thermal parameters for Pb with good improvements in the agreement factors

Table 1 Refined parameters after Rietveld refinement of PFN ND data at 290 K for nuclear structure, $a = 5.6802$ (5) Å, $b = 5.6723$ (4) Å, $c = 4.0273$ (4) Å, $\alpha = \gamma = 90.00°$ (0), $\beta = 89.820°$ (8); $R_p = 9.96$, $R_{wp} = 13.8$, $R_{exp} = 4.59$, $R_B = 6.59$ ($\chi^2 = 9.0$)

Atom	Wyckoff position	x	y	z	U_{eqv} (in Å^2)
Pb	1a	−0.0002	0.0000	0.0370	0.0327
Fe	1b	0.4968	0.0000	0.4832	0.0380
Nb	1b	0.4968	0.0000	0.4832	0.0380
O_1	1b	0.4702	0.0000	−0.0387	0.0389
O_2	2c	0.2394	0.2599	0.4536	0.0216

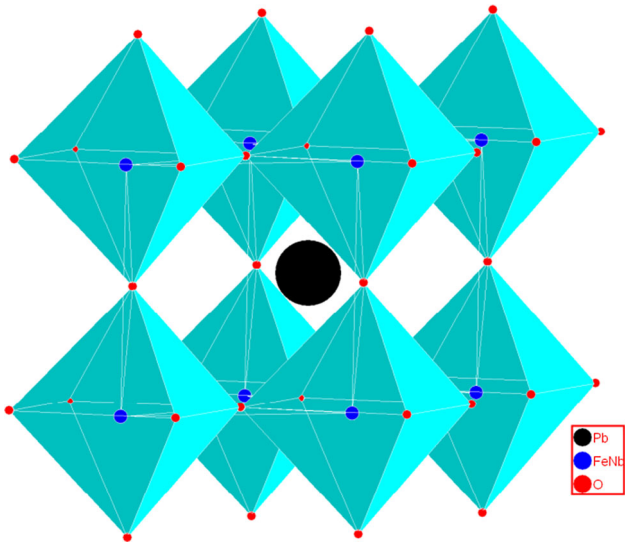

Fig. 2 A polyhedral view of the monoclinic perovskite structure of $Pb(Fe_{0.5}Nb_{0.5})O_3$ at room temperature

(Table 1). However, when we consider anisotropy for all the atoms of PFN (Pb, Fe, Nb, and O), further improvements were observed with reasonable *R* factors. In view of this, the atomic thermal motions were refined anisotropically while refining monoclinic structure [17, 18]. In the monoclinic phase with *Cm* space group, there are four atoms in the asymmetric unit with Pb, Fe/Nb, O_1 and O_2, in this Pb (1a) sites at (0,0,0), Fe, Nb, and O_1 in (1b) sites at (x, y, z), and O_2 in (2c) (x, 0, z) (Table 1). A polyhedral view of the monoclinic structure of PFN at room temperature is shown in Fig. 2.

Temperature-dependent crystallographic structure

Powder neutron diffraction study was performed on PFN at various temperatures in order to gain microscopic understanding of crystallographic structural parameters, across the Néel temperature (155 K). ND patterns of PFN were recorded at few selected temperatures 290, 180, 140, 120, 100, 50, 10, and 2 K across the Néel temperature. With

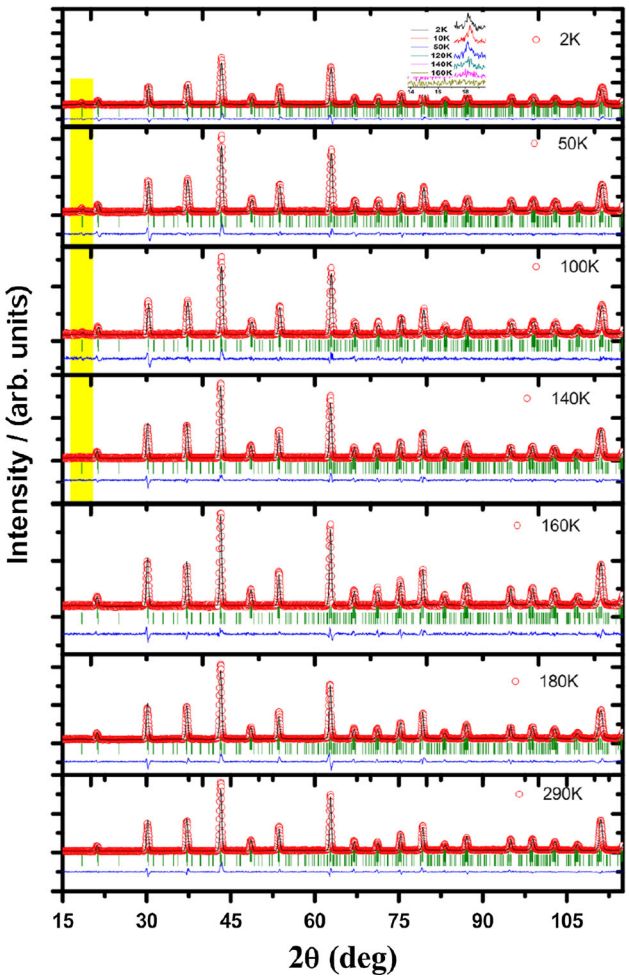

Fig. 3 The observed (*circles*) and calculated (*line*) neutron diffraction pattern for $Pb(Fe_{0.5}Nb_{0.5})O_3$ at different temperatures. Highlighted region shows the origin of AFM phase (T_N). Lower solid line is the difference between observed and calculated pattern. The first row of tick marks indicates the position of chemical Bragg peaks and second row indicate the position of magnetic Bragg peaks. Inset shows the ND patterns of sintered PFN at few selected temperatures and at selected 2θ range showing antiferromagnetic peak at 18.36° ($Q = 1.35$ Å^{-1})

decrease in temperature, a new magnetic peak appears at scattering vector, $Q = 1.35$ Å^{-1} (18.36° in 2θ), clearly indicates the emergence of antiferromagnetic order in the

system below 155 K. The inset of Fig. 3 shows the emergence of the magnetic peak below 155 K.

The Rietveld refinements of the temperature-dependent ND data were carried out considering only nuclear structure for $T > 155$ K (T_N) and both nuclear and magnetic structures for $T < 155$ K. The refinements using monoclinic structure showed good fitting with better R factors indicating an isostructural phase transition across the T_N from paramagnetic to antiferromagnetic phase. Figure 3 shows the Rietveld refinement plots of the ND data at few selected temperatures. The results of the Rietveld refinements, evolution of lattice parameters, cell volume, reliability factors (R factors), and χ^2 values along with bond distances, bond angles, and magnetic moments obtained after the refinements are shown in Table 2. The optimum and reasonable fitting of the diffraction data (expressed by the minimum R values) for all the measured temperatures was obtained for an antiferromagnetic G-type magnetic structure (Fig. 4).

Figure 4 shows the G-type magnetic structure; here every Fe cation is coupled anti-ferromagnetically to its nearest neighbors through Fe^{3+}–O–Fe^{3+} exchange interaction. The refined value of the magnetic moment for the Fe cations at 2 K is 2.00 μ_B, which is smaller than the spin-only moment of Fe^{3+} ($\mu_{eff} = 2\sqrt{(S(S+1))} = 5.9\ \mu_B$). This deviation suggests that the simple antiferromagnetic model adopted is only an approximation. This can be understood as due to the disorder of Fe^{3+} and Nb^{5+} ions at B sites, which lead to the variation in the strengths of the exchange interactions throughout the material. At places where the diamagnetic Nb^{5+} concentrations are more, it is expected that the antiferromagnetic coupling weakens. Thus, the obtained magnetic moment is an average value with the simple antiferromagnetic model considered. At the same time, this value is in reasonable agreement with the magnetic moments of Fe found previously in magnetically ordered Pb perovskites [14, 19–21]. The crystal structure of PFN corresponds to that of a B-site disordered perovskite, in which the Fe and Nb cations are distributed at random in the octahedral positions. Thus only 50 % of these sites are occupied by the magnetic Fe^{3+} ions. It is likely that the strength of the antiferromagnetic interaction is severely reduced both by the disordered spatial distribution of the Fe ions and by the dilution caused by diamagnetic Nb cations. Figure 5 shows the variation of magnetic moment with temperature from 2 to 295 K, the large drop in the magnetic moment at around 155 K corresponds to the transition (T_{N1}) from antiferromagnetic state to the paramagnetic state. The dip at 10 K might be due to another antiferromagnetic transition with weak ferromagnetic or spin-glass phase (T_{N2}). Inset of Fig. 5 shows the change in magnetic peak intensity at 10 K compare to 2 and 50 K data, this is well supportive for the magnetic moment versus temperature data (Fig. 5).

Figure 6 shows the (a) unit cell volume and (b) lattice parameters of PFN as a function of temperature. All the three lattice parameters a, b, and c show anomalies around 155 K, which is close to the magnetic transition temperature (T_N) reported in the literature [22]. It is evident from this figure that the monoclinic angle (β) decreases nonlinearly with increasing temperature. With the increase of temperature from 2 to 10 K, β decreases abruptly, may be due to the transition to the spin-glassy state as it is evident from the magnetic data (Fig. 9a) which will be discussed later. Further increase of temperature above 10 K, β shows a small variation until around 150 K (T_N), then it shows a small decrease up to 250 K and near RT it again increases. The overall change in β is very small and is in between 89.5° and 89.95°. The lattice parameter b becomes nearly temperature independent below 155 K, whereas lattice parameters a and c exhibit slight negative thermal expansion below T_N and shows a sudden expansion at the T_N. Similarly, the volume of the unit cell initially show no variation up to around 155 K, and then starts to increase above 155 K, showing a large volume thermal expansion at T_N. This kind of behavior with negative thermal expansion below the T_N (155 K) and an expansion above T_N was reported by Singh et al. [2]. The observed anomaly of lattice parameters across T_N is an indication of direct spin–lattice coupling in PFN multiferroic.

Figure 7 shows the temperature-dependent positional coordinates (a) x and z of Pb, (b) x and z of Fe/Nb, (c) x and z of the O_1, and (d) x, y, z of O_2 atoms in the unit cell obtained from the Rietveld refinements of neutron diffraction data taken at different temperatures (290–2 K). The Pb and O_1 atomic positions exhibit anomalies around T_N. Keeping the Cm space group and with the propagation vector $k = [0.125, 0.5, 0.5]$ constant during the refinement, the observed anomalies across the T_N suggests that the change of atomic positions occur due to an isostructural phase transition at 155 K. In isostructural phase transition, there is no change in the space group and Wyckoff positions across the T_N. The dotted vertical line shows the anomalies around the magnetic transition at 155 K (T_N). The observed anomaly of atomic positions across T_N is an indication of direct spin–lattice coupling. In comparison with the earlier reports of large scattering in T_N, from 143 to 200 K [2, 10, 11, 23, 24], the observed value 155 K is within the range of reported values.

Magnetic structure refinement (at $T = 2$ K)

Figure 8 Shows the Rietveld refined ND data taken at 2 K, refinement done for both nuclear and magnetic structures with monoclinic structure (Cm space group). In the analysis of structural part (nuclear structure), no extra peaks or splitting of main reflections were observed. The (1 0 0/1 1 0) magnetic peak intensity was increased at 2 K compared

Table 2 Reliability factors of ND data refinement for PFN from 2 to 290 K with *Cm (monoclinic)* space group for nuclear structure

Parameters	2.8 K	10 K	50 K	100 K	120 K	140 K	160 K	180 K	205 K	250 K	255 K	290 K
Space group	*Cm* symmetry with monoclinic phase											
a (Å)	5.6732 (5)	5.6688 (6)	5.6688 (6)	5.6687 (7)	5.6683 (8)	5.6870 (4)	5.6825 (3)	5.6859 (3)	5.6821 (4)	5.6826 (3)	5.6824 (4)	5.6802 (5)
b (Å)	5.6602 (5)	5.6611 (6)	5.6638 (6)	5.6655 (7)	5.6648 (7)	5.6668 (2)	5.6702 (2)	5.6678 (2)	5.6726 (3)	5.6733 (3)	5.6733 (2)	5.6723 (4)
c (Å)	4.0176 (3)	4.0166 (3)	4.0168 (3)	4.0167 (4)	4.0172 (4)	4.0307 (3)	4.0316 (3)	4.0340 (3)	4.0356 (4)	4.0349 (3)	4.0316 (3)	4.0273 (4)
β (°)	89.798 (1)	89.743 (8)	89.730(6)	89.739 (8)	89.755 (9)	89.755 (7)	89.732 (6)	89.754 (6)	89.693 (7)	89.711 (6)	89.745 (6)	89.820 (8)
Volume $(Å)^3$	129.009 (2)	128.903 (2)	128.968 (2)	128.997 (3)	128.992 (3)	129.901 (1)	129.902 (1)	130.005 (1)	130.075 (2)	130.083 (1)	129.970 (1)	129.758 (2)
R_p (%)	8.01	4.92	7.81	7.47	10.6	8.56	4.58	7.05	6.92	7.21	5.06	9.96
R_{wp} (%)	10.5	6.56	10.7	9.77	14.3	11.1	5.95	9.10	8.90	9.37	6.65	13.8
R_{exp} (%)	4.62	3.65	4.59	5.49	4.11	4.06	3.14	3.16	4.47	3.34	3.72	4.59
χ^2	5.18	3.22	5.42	3.17	12.1	7.49	2.67	8.29	3.96	7.88	3.19	9.00
Brag *R* factor	5.90	4.83	5.24	7.13	6.42	5.35	5.17	6.57	6.36	8.11	6.05	6.59
R_f factor	2.50	2.25	2.37	3.87	3.29	2.82	2.85	3.23	3.46	5.45	3.01	3.24
Selected bond lengths												
Average Pb–Fe/Nb (Å)	3.3534	3.3500	3.3496	3.3498	3.3502	3.4035	3.4871	3.4165	3.4566	3.4097	3.4307	3.3708
Average Pb–O1 (Å)	3.1025	3.1005	3.1005	3.1003	3.1001	2.9697	3.2068	3.1793	3.1777	3.1063	3.1313	3.0246
Average Pb–O2 (Å)	3.0253	3.0236	3.0237	3.0240	3.0244	2.8043	2.9660	2.9774	2.9771	3.0059	3.0313	3.0868
Selected bond angles												
Average Pb–Fe–Nb (°)	32.819 (10)	32.848 (9)	32.853 (9)	32.851 (11)	32.851 (12)	33.848 (7)	1.984 (6)	1.480 (6)	1.482 (7)	34.659 (7)	33.905 (7)	32.220 (8)
Magnetic structure												
Mag *R* factor	65.1	75.1	50.6	70.01	63.5	68.2	73.3	74.99	85.4	88.9	89.1	80.8
Propagation vector, k	[0.125, 0.5, 0.5]											
Magnetic moments												
μ_{AFM}	2.00	1.41	2.01	2.02	2.00	0.90	0.72	0.72	0.73	0.79	0.73	0.73

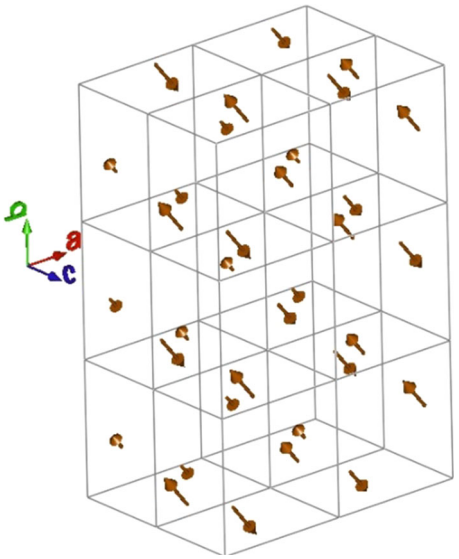

Fig. 4 Schematic representation of the G-type magnetic structure, indicating a monoclinic unit cell with doubled axes

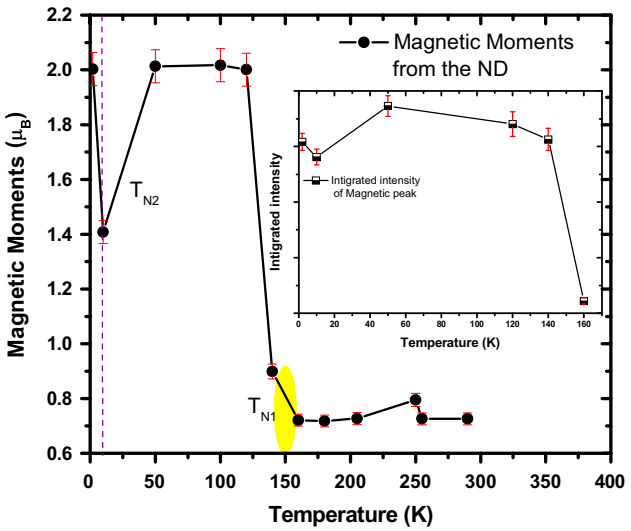

Fig. 5 Variation of magnetic moment as a function of temperature. Inset shows the variation of integrated intensity of magnetic peak with temperature

to the data at higher temperatures. In order to determine the magnetic structure, a propagation vector, $k = [0.125, 0.5, 0.5]$ considering Fe as a lone magnetically active ion and a two-phase refinement was performed. The inset of Fig. 8 shows the zoomed part of the magnetic peak region which occurred at $2\theta = 18.33°$ showing a good fit of the data. Table 3 shows the final refined parameters for magnetic and nuclear structures at 2 K.

Magnetization studies

The magnetic susceptibility measurements in zero-field cooled (ZFC) and field-cooled (FC) modes, were carried

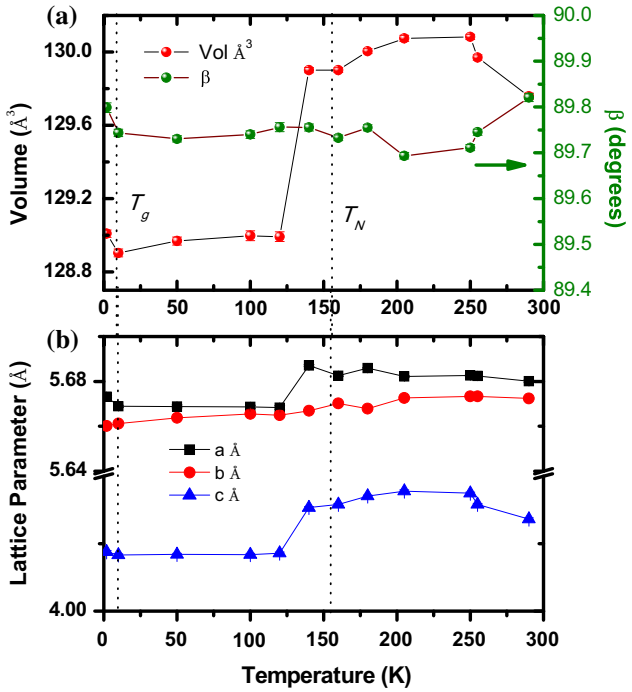

Fig. 6 Temperature-dependent variation of **a** unit cell volume and β **b** lattice parameters a, b, and c obtained from Rietveld refinements using powder Neutron diffraction data

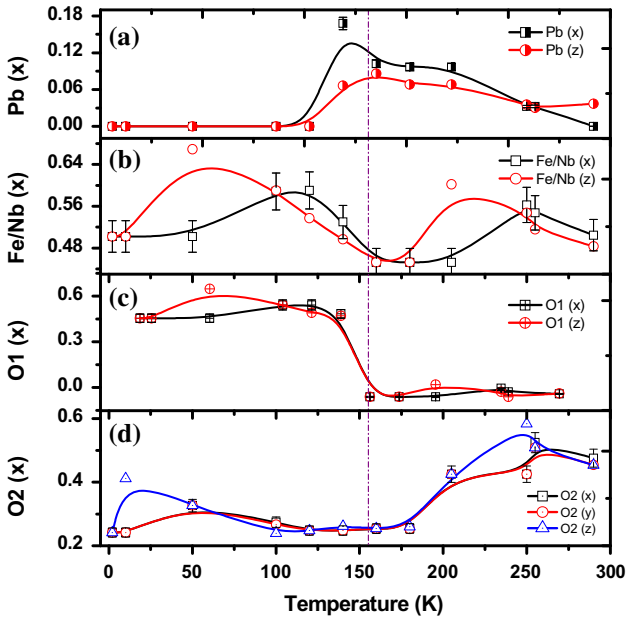

Fig. 7 Temperature-dependent positional coordinates **a** x and z of Pb **b** x and z of Fe/Nb **c** x and z of the O_1, and **d** x, y, and z of O_2 atoms in the unit cell obtained from the Rietveld refinements using temperature-dependent neutron diffraction (290–2 K). The dotted vertical line shows the anomalies around the magnetic transition at 155 K (T_N)

out from 5 to 400 K on PFN. The thermal evolution of the magnetic susceptibility ($\chi = M/H$) of PFN measured in both zero-field cooled (ZFC) and field-cooled (FC) modes in a field of 500 Oe is shown in Fig. 9a. The ZFC curve increases monotonically on decreasing temperature from 300 K, and exhibits a cusp around 155 K (T_{N1}), indicating the onset of antiferromagnetic ordering. However on further decrease in temperature, χ increases further and exhibits another peak around 10 K (T_{N2}) before falling rapidly as T approaches to 5 K. The FC curve also show similar features at $T > 10$ K, however the feature seen in ZFC below 10 K is not observed in FC, as the moment is still increasing as T approaches 5 K. It must be noticed here that there is a very clear bifurcation in ZFC and FC curves above 155 K (i.e., T_N), which indicates magnetic anisotropy in this system which appears well above T_N. The ZFC–FC bifurcation also exhibits local clustering of the spins [23] or anti/ferromagnetic domain growth [24]. Therefore, in the ZFC curve the peak around 10 K can be interpreted in terms of spin-glass transition or freezing of domain-wall motion [25]. The ZFC–FC curves merge around 380 K. It may be recalled here that, the ferroelectric

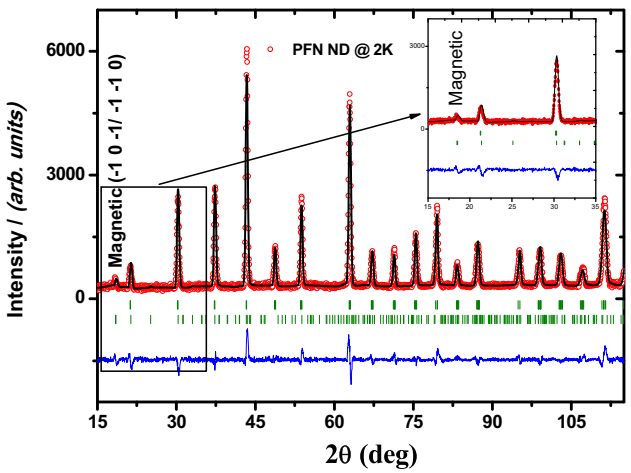

Fig. 8 Rietveld refined Neutron diffraction data at 2 K. Inset shows the magnetic peak at $2\theta = 18.36°$ ($\lambda = 1.48$ Å)

Curie temperature (T_C) is reported to be around 370–380 K [23, 26]. The ferroelectric phase transition might influence the magnetic susceptibility, which results in a magnetic anomaly at 380 K. Our susceptibility measurement results are in good agreement with the reported results [23].

FC and ZFC curves around 10 K shows distinct divergence, which could be related to the origin of some kind of freezing phenomenon giving rise to spin-glassy phase or cluster-glass state. Similar behavior was reported by Kleemann et al. [27] and Laguta et al. [28] mentioning that number of different parameters is involved. Studies of 93Nb NMR spectra of PFN revealed the presence of Fe rich, Nb poor as well as Fe poor, and Nb rich regions. The first ones are likely to form the AFM regions while in the latter the spin-glass (or cluster-glass)-type state is most probable [28]. Generally, in Pb-based systems, spin cluster-glass (CG) phase coexists with antiferromagnetic (AF) long-range order as conjectured previously [29]. The AF state occupies the percolating exchange-coupled Fe^{3+} cluster; while the CG state comprises rare isolated Fe^{3+} ions and unblocked super antiferromagnetic (SAF) Fe^{3+} clusters with uncompensated magnetic moments [30, 31]. Recently, Chillal et al. confirms the homogeneous co-existence of AF and SG ordering based on neutron and Mossbauer spectroscopy [32]. It clearly reveals an anomaly around 155 K characteristic of an AFM transition and below 10 K spin-glassy phase or cluster-glass state. Figure 9b shows inverse susceptibility graph, $1/\chi$ versus temperature, exhibiting the similar anomalies at 155 and 10 K. The paramagnetic Curie temperature (θ_p) and the effective Bohr magnetron number (μ_{eff}) were estimated from the fit of Curie–Weiss law given by,

$$\chi = \frac{C}{T - \theta_p},$$

where C is Curie constant, θ_p is paramagnetic Curie temperature. The obtained values of θ_p and μ_{eff} are −149.46 K and 3.10 μ_B/f.u., respectively. Figure 9c shows isothermal magnetization-field (M-H) curves measured at different temperatures. From these data, it is possible to observe a very small opening of hysteresis loop at below 120 K with

Table 3 Final refined parameters for magnetic and nuclear structures at 2 K, $a = 5.6732(5)$ Å, $b = 5.6602(5)$ Å, $c = 4.0176(3)$ Å, $\alpha = \gamma = 90.00°$, $\beta = 89.798(1)°$; $R_p = 8.01$, $R_{wp} = 10.5$, $R_B = 5.90$

Atom	Wyckoff position	x	y	z	Ueqv (in Å^2)
Pb	1a	0.0000	0.0000	0.0000	0.0269
Fe	1b	0.5021	0.0000	0.4523	0.0106
Nb	1b	0.5021	0.0000	0.4523	0.0106
O_1	1b	0.4550	0.0000	−0.0615	1.9416
O_2	2c	0.2416	0.2475	0.4251	0.4398

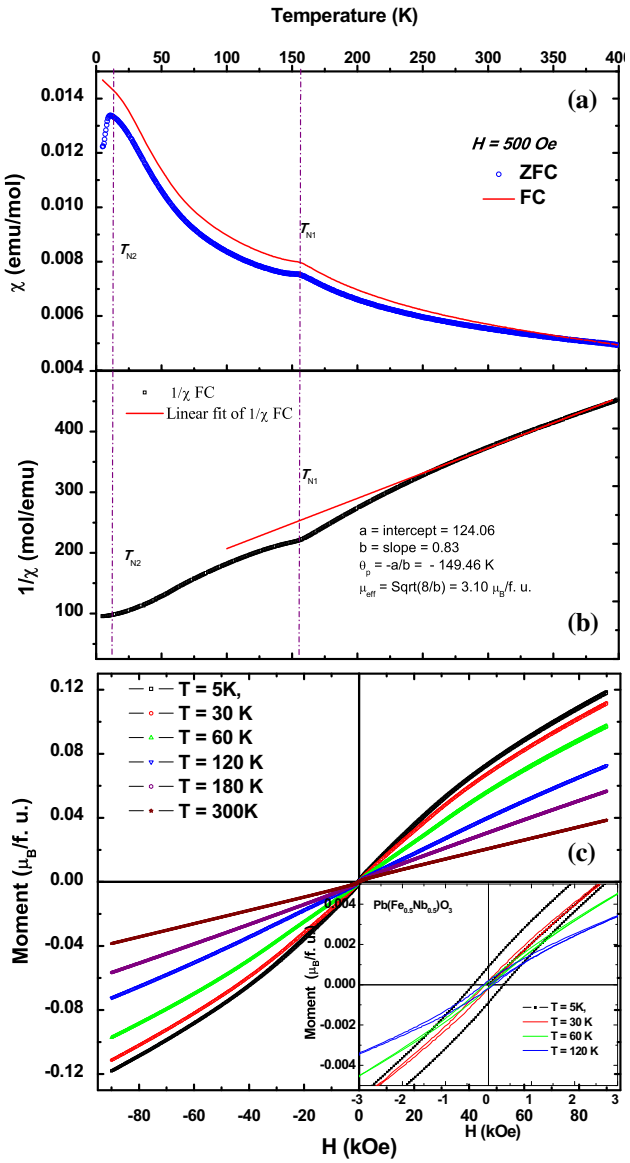

Fig. 9 Variation of **a** magnetic susceptibility (ZFC and FC curves) with temperature measured at 500 Oe, **b** inverse susceptibility with temperature at 20 kOe (recorded in FC mode), **c** magnetization (M) with applied magnetic field (H) hysteresis loops of PFN at various temperatures above and below the T_N (**c**). The inset of (**c**) shows the M–H loops at 5 K

little coercive field (0.12 kOe). However, the hysteresis loop measured at 5 K shows clear opening of the loop with increase of the coercive field (0.36 kOe) and the remnant magnetization (8.75×10^{-4} emu/gm), suggesting the presence of a possible canting in the coupled magnetic moments. Similar results were reported by Laguta et al. [33], where the considerable remanent magnetization observed at around 5 K decreases with increase in temperature. The temperature dependence of observed remnant magnetization (M_r), saturation magnetization (M_s), and coercive field (H_c) are shown in Table 4.

Evidence of direct coupling between the electric and magnetic ordering through measurements of polarization versus electric field: ferroelectric studies.

To study the direct coupling between the electric and magnetic ordering, measurements of polarization versus electric field at low temperatures were carried out using cryogenic 20 K closed cycle refrigerator system with a temperature uncertainty of ±5 K. Figure 10 shows the ferroelectric hysteresis loops measured at different temperatures from 100, 130, 150, 200, 250, and 300 K, with maximum field value of (E_{max}) 15 kV/cm. At low temperatures (100, 130, and 150 K), hysteresis loops appear to be quasi linear and tend to show near hysteretic behavior at higher temperatures [34]. The quasi-linear nature of the hysteresis curves is due to the slight conducting nature of the samples. The inset (a) of Fig. 10 shows variation of saturation polarization (P_s) and remnant polarization (P_R) with temperature, which clearly show a sudden increase after T_N. The area under the hysteresis curve, corresponds to the dissipation energy or loss, gives the indirect information about the conductivity of the sample. The areas under the hysteresis curves from Fig. 10 are estimated.

Figure 11 show the temperature dependence area of the hysteresis loop versus 1000/T plot (Arrhenius plot). An interesting anomaly, change in the slope, is observed around 155 K (near T_N). The activation energy (E_{act}) values obtained below and above the T_N are 0.0062 and 0.074 eV, respectively. The difference between the E_{act} values below and above T_N, can be explained by the occurrence of a symmetry change depending on the degree of ordering of Fe^{3+} and Nb^{5+} ions over B-site in good agreement with the previous reports on structural studies carried out using Rietveld refinement method on neutron and X-ray diffraction data for powders around this low temperature region [12, 14]. Here, change in the electrical polarization behavior can be promoted by the transition from an ordered and less ferroelectric monoclinic structure at ($T < T_N$), where the Fe^{3+} ions at the B-site form a antiferromagnetic array to a B-site disordered and highly ferroelectric monoclinic structure (at $T > T_N$), when it becomes paramagnetic. Moreover, these slope changes are in correspondence with the dielectric anomaly observed from measurements of dielectric constant and dielectric loss near 155 K, assumed as evidence of the magneto-electric coupling by Gao et al. [35] in PFN ceramic samples and by Yang et al. [36] in PFN crystals, where coincidence with theoretical predictions was found.

Evidence for magneto-electric coupling: dielectric studies

The dielectric measurements were performed as a function of temperature, from 7 to 350 K, on a sintered pellet of PFN. The dielectric constant (ε) measured as a function of

Table 4 Remnant magnetization (M_r), saturation magnetization (M_s), and coercive field (H_c) of PFN at different temperatures

Temperature (K)	Remnant magnetization (M_R) (emu/gm)	Saturation magnetization (M_{max}) (emu/gm)	Coercive field (H_c) (kOe)
5	8.75×10^{-4}	0.12	0.36
30	1.99×10^{-4}	0.11	0.08
60	1.70×10^{-4}	0.10	0.10
120	2.05×10^{-4}	0.07	0.13
180	2.24×10^{-4}	0.05	0.16
300	3.05×10^{-4}	0.04	0.30

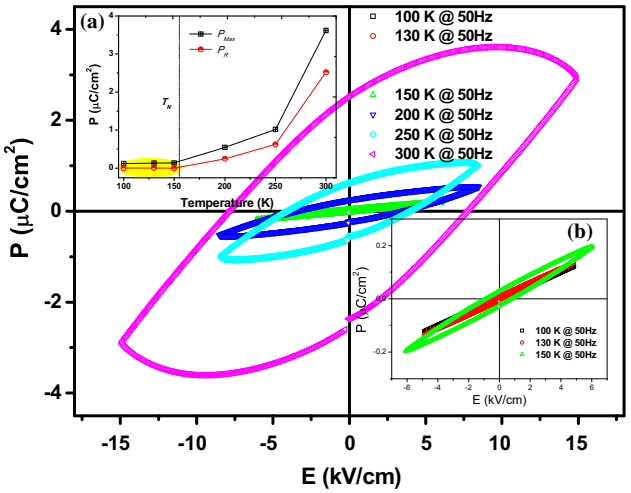

Fig. 10 Ferroelectric *P-E* loops measured at 100, 130, 150, 200, 250, and 300 K. Top left inset (**a**) temperature dependence of P_{Max} and P_R. Bottom right inset (**b**) low temperature quasi-linear loops (100–150 K)

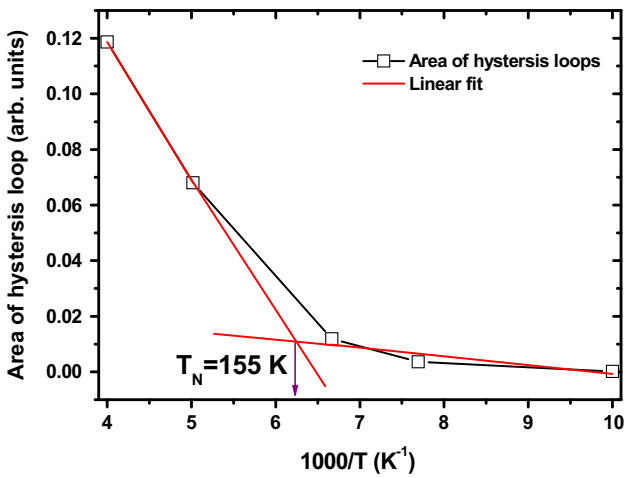

Fig. 11 Arrhenius plots of area under the ferroelectric *P–E* hysteresis loops at above and below T_N

temperature at 0.5–100 kHz are shown in Fig. 12. Temperature-dependent dielectric behavior is broadly consistent with the previous reports on PFN [36].

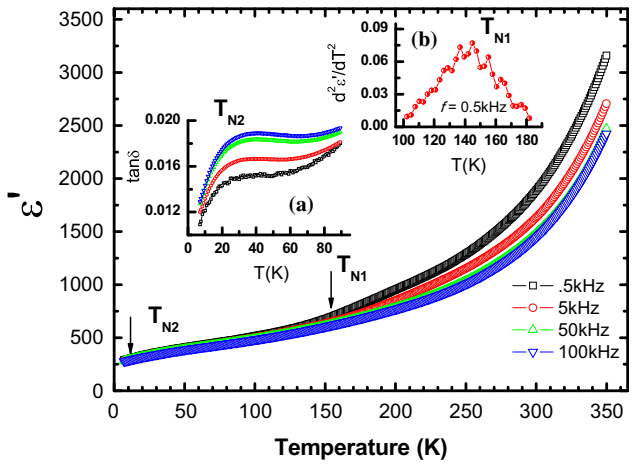

Fig. 12 Dielectric constant with temperature at different frequencies (0.5 to 100 kHz). The inset (**a**) show the Dielectric loss (tanδ) with temperature and inset (**b**) show the $d^2\varepsilon'/dT^2$ with temperature

The $\varepsilon(T)$ does not show much variation till T_N (155 K) and exhibits an abrupt change above T_N followed by a frequency dispersion. The anomaly can be seen in terms of change in the slope of the curve around T_N, which is more pronounced at lower frequencies than at higher frequencies. This transition/anomaly can be seen clearly in $d^2\varepsilon'/dT^2$ plot with temperature for 0.5 kHz (inset (b) of Fig. 12). The onset of anomaly shifts from 134 K for 0.5 kHz to 158 K at 100 kHz on increasing the measuring frequency, with a concomitant decrease in the value of the dielectric constant, mimicking a relaxor ferroelectric behavior. A large increase in the dielectric loss is observed along with frequency dispersion above T_N. Also such anomaly in $\varepsilon(T)$ around T_N has been reported by others literature in PFN material itself. Yang et al. [36] showed a jump in dielectric constant (as like in our results) at near T_N (143 K) in PFN single crystals and correlated to the coupling between ferroelectric and magnetic orders in PFN. The $\delta\varepsilon$ (change in dielectric constant) was correlated to M^2 (square of magnetic order parameter). Correa et al. [37], observed an anomaly in dielectric constant at around 170 K in PFN thin films and correlated to the weak magneto-

electric coupling, further showed that, the change in dielectric constant ($\delta\varepsilon$) is proportional to the square of magnetic order parameter. Similarly, Lente et al. [38] through microwave dielectric measurements, showed a clear dielectric anomalies (a peak in $\Delta\varepsilon$ and a local minimum for f_R) around 149 K (T_N) and propose that the magneto-electric coupling in PFN takes place indirectly via ferroelastic contribution. This in fact, corroborates well with our results shown in Fig. 6, a signature of spin–lattice coupling. In another report, Correa et al. [39] have showed the phonon anomalies (through Raman studies) and the lattice parameter anomalies in the vicinity of T_N, which was correlated to spin-phonon coupling. Such correlations have been reported in many other AFM materials, such as $TbMnO_3$, $YMnO_3$, $HoMnO_3$, and $0.9BiFeO_3$–$0.1BaTiO_3$ [40–43]. Other possible reason for the observed dielectric anomaly being Maxwell–Wagner type of relaxation or relaxation associated with oxygen vacancies as observed by Raevski et al. [44, 45] in similar non-Pb-based materials.

Another interesting dielectric anomaly was observed at around 20 K both in dielectric constant and dielectric loss (see the inset (a) of Fig. 12), similar to the ND results presented in Figs. 5, 6, and 7, as well as magnetic susceptibility results presented in Fig. 9a. This anomaly could be related to another magnetic transition (T_{N2}) such as spin-glass transition.

Atomic level evidence for linear magneto-electric coupling

The increasing dielectric constant at all the frequencies above T_N as discussed above and shown in Fig. 12, clearly suggests modification of the lattice polarization in magnetically ordered state. As seen from Fig. 6b, a drastic change in the lattice volume observed across the magnetic phase transition (T_N) which will alter the polarization of the material. Figure 7 shows the temperature-dependent atomic positional coordinates of all the atoms in the asymmetric unit as obtained by Rietveld refinement analysis of neutron diffraction data and discussed earlier. It is clearly evident from this figure that the atomic positions show noticeable anomaly across T_N for both the cations and anions. Changes in atomic positions are consistent with the earlier report [2, 45]. The changes in atomic positions are due to an isostructural phase transition accompanying the magnetic transition around 155 K. We calculated ionic polarization of PFN from the refined atomic positions. Calculated ionic polarization of PFN under point charge approximation at different temperatures is shown in Fig. 13. The octahedral tilt angle distortions in perovskites first introduced by Glazer [46] and the detailed explanation on this can be found in the original article [46].

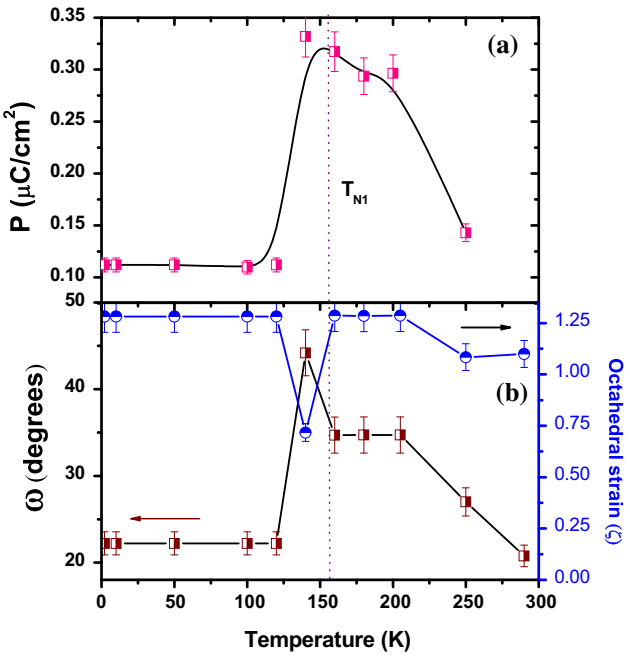

Fig. 13 Temperature dependence of the (**a**) ionic polarization calculated using atomic positional coordinates of $Pb_{x,y,z}$, $Fe/Nb_{x,y,z}$ and $O_{x,y,z}$ atoms (**b**) octahedral tilt angle (left side) calculated using positional coordinates of the O_x and O_y atoms and right side arrow shows octahedral strain (ζ). The doted curve shows anomaly at T_N, polarization and tilt angle

From the obtained information about the atomic positions from 2 to 290 K with very high accuracy, we can study how electric charge distribution, i.e., electric dipole moments, evolve as a function of temperature. We assigned nominal charge values for Pb^{2+}, Fe^{3+}, Nb^{5+}, and O^{2-} for our calculations [47]. Although, we acknowledge that this assumption of nominal charge assignment may be oversimplified, nevertheless we believe that our calculation captures the essential temperature variations of the charge distribution inside the unit cell. The use of more realistic charge values would alter our results only quantitatively. After ensuring that we satisfied the charge neutrality inside the unit cell, then we calculated the dipole moments based on the aforementioned model [48]. In our calculation *x*, *y*, and *z* atomic coordinates are considered zero at 2 K. When we started refinement at different temperatures, the atomic coordinates are changed significantly. Temperature dependent *x*, *y*, and *z* coordinates show increase in the polarization around T_N. When we take average polarization (Fig. 13a) along *x* axis, *y* axis, and *z* axis, we observed a large change in polarization around T_N. This large change in polarization observed around T_N (at 155 K) corroborates with the results observe in *P*–*E* loops and $\varepsilon(T)$. This observation of change in polarization around T_N is may be an indicative of a coupling between the electric and magnetic dipole moments. The polarization values (Fig. 13a)

calculated from neutron data are comparable to those of experimentally observed values (Fig. 10) at low temperatures (below T_N) and above T_N they differ by about one order of magnitude. However, our results, both experimental and calculated from ND are about two orders of magnitude lower compared to those reported in literature, from the first principle calculation (0.55–0.60 C/m^2) [49] and observed experimentally for highly resistive ceramics (0.25–0.30 C/m^2) [50]. The difference may be due to the conducting nature of the samples.

Its more interesting that not only ionic polarization changes around the T_N, but also the octahedral tilt angle as shown in Fig. 13b, which confirms the isostructural phase transition [47]. Octahedral tilt (ω) and strain (ζ) are the very important parameters in perovskite (ABO_3)-structured materials; slight octahedral distortions have close links to the functional properties. The octahedral tilt angle (ω) was calculated using the expression.

$$\omega = \tan^{-1} 4\sqrt{3}e,$$

where 'e' is determined from the oxygen atomic positions [46, 47]. The tilt angle and the monoclinic cell parameters are coupled through an additional parameter called the octahedral strain (ζ) [47, 48, 51].

Conclusions

In summary, the multiferroic PFN was synthesized by single-step method using lower calcination and sintering temperatures. The 100 % perovskite phase with no traces of pyrochlore phase was obtained. The room temperature XRD and Neutron diffraction studies showed that the synthesized PFN is in the monoclinic phase with space group *Cm*. The complex controversial structure was probed using powerful tool of temperature-dependent powder neutron diffraction technique. Through ND studies between 290 and 2 K, the magnetic transition (T_N) was observed at around 155 K with G-type antiferromagnetic ordering and is in agreement with the earlier reports. There was no change in crystallographic symmetry even below 155 K; monoclinic (*Cm* space group) structure remains in the entire temperature range of measurement. Thermal expansion anomaly was observed through the well-distinguishable changes in unit cell volume across the T_N. Two anomalies were found in temperature-dependent magnetization. The first was attributed to the PM-to-AFM transition at T_{N1}. Anomaly at around T_{N2} (10 K) is probably caused by the transition to the spin-glass state, but on the basis of the present measurements, this conclusion is not sufficient. Further investigation is required to confirm low temperature magnetic phase. *M–H* loops well supports the ZFC and FC susceptibility patterns. We investigated the temperature-dependent *P-E* loops, changes in the electrical polarization behavior were observed during the occurrence of a paramagnetic to weakly magnetized antiferromagnetic transition near 155 K. Consistent to magnetic measurements, two anomalies are also observed in the dielectric permittivity around T_{N1} and at 20 K (T_{N2}). This behavior is a clear evidence of intrinsic magneto-electric coupling.

Significant change in the atomic positions was observed above the magnetic transition (T_{N1}). The calculated ionic polarizations show clear evidence of atomic level magneto-electric coupling phenomenon. Total spontaneous polarization shows enhancement in polarization around T_{N1}. The ionic polarization and octahedral tilt angle shows the anomaly confirming the first-order character of the isostructural phase transition. It also reveals the presence of magneto-electric coupling. Our present study thus provides convincing explanation for the origin and presence of magneto-electric coupling in PFN and classifying it as a potential multiferroic material.

Acknowledgements Authors (SM and BA) would like to acknowledge UGC-DAE-CSR, Mumbai for financial support through the project CRS-M-159. Authors thank Prof. E. V. Sampathkumaran, TIFR, Mumbai, India for the dielectric measurements, also they are thankful to UGC-DAE CSR Indore for providing ferroelectric measurement facility.

References

1. Cheong S-W, Mostovoy M (2007) Multiferroics: a magnetic twist for ferroelectricity. Nat Mater 6:1–20
2. Singh SP, Pandey D, Yoon S, Baik S, Shin N (2007) Evidence for monoclinic crystal structure and negative thermal expansion below magnetic transition temperature in Pb(Fe1/2Nb1/2)O3. Appl Phys Lett 90:242915-1–24915-3
3. Brunskill IH, Schmidt H, Tissot P (1981) The characterrization of high temperature solution-grown crystals of Pb($Fe_{1/2}$ $Nb_{1/2}$)O3. Ferroelectrics 37:547–550
4. Bokov AA, Emelyanov SM (1991) Electrical properties of $Pb(Fe_{0.5}Nb_{0.5})O_3$ crystals. Phys Status Solidi B 164:K109–K112
5. Bonny V, Bonin M, Sciau P, Schenk KJ, Chapuis G (1997) Phase transitions in disordered lead iron niobate: X-ray and synchrotron radiation diffraction experiments. Solid State Commun 102:347–352
6. Yasuda N, Ueda Y (1989) Dielectric properties of $PbFe_{1/2}Nb_{1/2}O_3$under pressure. Ferroelectrics 95:147–151
7. Yokosuka M (1993) Electrical and electromechanical properties of hot-pressed $Pb(Fe_{1/2}Nb_{1/2})O_3$ ferroelectric ceramics. Jpn J Appl Phys 32:1142–1146
8. Fu SL, Chen CF (1989) Fabrication of perovskite $Pb(Fe_{1/2}Nb_{1/2})O_3$and reaction mechanism. Ferroelectrics 82:119–126
9. Smolenskii GA, Agranovskaia AI, Popov SN, Isupov VA (1958) Sov Phys Tech Phys 3:1981
10. Singh SP, Singh AK, Pandey D (2007) Evidence for a monoclinic M_A to tetragonal morphotropic phase transition in (1-x) $Pb(Fe_{1/2}Nb_{1/2})O_3$– x $PbTiO_3$ ceramics. J Phys 19:036217-1–036217-9

11. Peng W, Lemee N, Karkut M, Dkhil B, Shvartsman VV, Borisov P, Kleemann W, Holc J, Kosec M, Blinc R (2009) Spin-lattice coupling in multiferroic $Pb(Fe_{1/2}Nb_{1/2})O_3$ thin films. Appl Phys Lett 94:012509-1–012509-3
12. Lampis N, Sciau P, Lehmann AG (1999) Rietveld refinements of the paraelectric and ferroelectric structures of $PbFe_{0.5}Nb_{0.5}O_3$. J Phys 11:3489–3500
13. Mabud SA (1984) X-ray and neutron diffraction studies of lead iron niobate ceramics and single crystals. Phase Trans 4:183–200
14. Ivanov SA, Tellgren R, Rundlof H, Thomas NW, Ananta S (2000) Investigation of the structure of the relaxor ferroelectric $Pb(Fe_{1/2}Nb_{1/2})O_3$ by neutron powder diffraction. J Phys 12:2393–2400
15. Bhat VV, Angadi B, Umarji AM (2005) Synthesis, low temperature sintering and property enhancement of PMN–PT ceramics based on the dilatometric studies. Mater Sci Eng B 116:131–139
16. Matteppanavar S, Angadi B, Rayaprol S (2013) Single phase synthesis and room temperature neutron diffraction studies on multiferroic $PbFe_{0.5}Nb_{0.5}O_3$. AIP Conf Proc 1512:1232–1233
17. Baldinozzi G, Sciau Ph, Lapasset J (1992) Crystal Structure of Pb_2 $CoWO_6$ in the Cubic Phase. Phys Status Solidi A 133:17–23
18. Singh AK, Pandey D, Zaharko O (2006) Powder neutron diffraction study of phase transitions in and a phase diagram of (1 − x)[Pb(Mg1/3Nb2/3)O3]-xPbTiO3. Phys Rev B 74: 024101-1–024101-18
19. Lampis N, Sciau P, Lehmann AG (2000) Rietveld refinements of the paraelectric and ferroelectric structures of $PbFe_{0.5}Ta_{0.5}O_3$. J Phys 12:2367–2378
20. Ivanov SA, Eriksson SG, Thomas NW, Tellgren R, Rundlof H (2001) A neutron powder diffraction study of the ferroelectric relaxor $Pb(Fe_{1/2}Ta_{1/2})O_3$. J Phys 13:25–34
21. Ivanov SA, Eriksson SG, Tellgren R, Rundlof H (2004) Neutron powder diffraction study of the magnetoelectric relaxor $Pb(Fe_{2/3}W_{1/3})O_3$. Mater Res Bull 39:2317–2328
22. Watanabe T, Kohn K (1989) Magnetoelectric effect and low temperature transition of $PbFe_{0.5}Nb_{0.5}O_3$ single crystal. Phase Transit 15:57–68
23. Havlicek R, Poltierova J, Vejpravova Bochenek D (2010) Structure and magnetic properties of perovskite-like multiferroic $PbFe_{0.5}Nb_{0.5}O_3$. J Phys 200:0120581–0120583
24. Vincent E, Dupuis V, Alba M, Hammann J, Bouchaud J-P (2000) Aging phenomena in spin-glass and ferromagnetic phases: domain growth and wall dynamics. Europhys Lett 50:674–680
25. Chang H, Guo Y-Q, Liang J-K, Rao G-H (2004) Magnetic ordering and irreversible magnetization between ZFC and FC states in RCo_5Ga_7 compounds. J Magn Magn Matter 278:306–310
26. Ashok Kumar, Katiyar RS, Carlos Rinaldi, Lushnikov Sergey G, Shaplygina Tatjana A (2008) Glasslike state in $Pb(Fe_{1/2}Nb_{1/2})O_3$ single crystal. Appl Phys Lett 93:232902
27. Kleemann W, Shvartsman VV, Borisov P (2010) Coexistence of Antiferromagnetic and Spin Cluster Glass Order in the Magnetoelectric Relaxor Multiferroic $Pb(Fe_{1/2}Nb_{1/2})O_3$. Phys Rev Lett 105:257202
28. Laguta VV, Rosa J, Jastrabik L, Blinc R, Cevc P, Zalar B, Remskar M, Raevskaya SI, Raevski IP (2010) ^{93}Nb NMR and Fe^{3+} EPR study of local magnetic properties of magnetoelectric $Pb(Fe_{1/2}Nb_{1/2})O_3$. Mater Res Bull 45:1720
29. Rotaru GM, Roessli B, Amato A, Gvasaliya SN, Mudry C, Lushnikov SG, Shaplygina TA (2009) Spin-glass state and long-range magnetic order in $Pb(Fe_{1/2}Nb_{1/2})O_3$ seen via neutron scattering and muon spin rotation. Phys Rev B 79:184430
30. Neel L, Acad. Sci. Paris C.R. 253, 9 (1961)
31. Larrégola SA, Pedregosa JC, Algueró M, Jimenez R, Garcia-Hernandez M, Fernandez-Diaz MT, Alonso JA (2012) A novel near-room-temperature type I multiferroic: $Pb(Fe_{0.5}Ti_{0.25}W_{0.25})O_3$ with coexistence of ferroelectricity and weak ferromagnetism. Chem Mater 24(14):2664–2672
32. Chillal S, Thede M, Litterst FJ, Gvasaliya SN, Shaplygina TA, Lushnikov SG, Zheludev A (2013) Microscopic coexistence of antiferromagnetic and spin-glass states. Phys Rev B 87: 220403(R)
33. Laguta VV, Glinchuk MD, Mary sko M, Kuzian RO, Prosandeev SA, Raevskaya SI, Smotrakov VG, Eremkin VV, Raevski IP (2013) Effect of Ba and Ti doping on magnetic properties of multiferroic $Pb(Fe_{1/2}Nb_{1/2})O_3$. Phys Rev B 87:064403
34. Font R, Alvarez G, Raymond O, Portelles J, Siqueiros JM (2008) Evidence of magnetodielectric coupling in multiferroic $Pb(Fe_{0.5}Nb_{0.5})O_3$ ceramics from ferroelectric measurements and electron paramagnetic resonance. Appl Phys Lett 93:172902-1–172902-3
35. Gao XS, Chen XY, Yin J, Wu J, Liu ZG, Wang M (2000) Ferroelectric and dielectric properties of ferroelectromagnet $Pb(Fe_{1/2}Nb_{1/2})O_3$ ceramics and thin films. J Mater Sci 35:5421–5425. doi:10.1023/A:1004815416774
36. Yang Y, Liu J-M, Huang HB, Zou WQ, Bao P, Liu ZG (2004) Magnetoelectric coupling in ferroelectromagnet $Pb(Fe_{1/2}Nb_{1/2})0O_3$ single crystals. Phys Rev B 70:132101-1–132101-4
37. Correa M, Kumar A, Katiyar RS, Rinaldi C (2008) Observation of magnetoelectric coupling in glassy epitaxial $PbFe_{0.5}Nb_{0.5}O_3$ thin films. Appl Phys Lett 93:192907-1–192907-3
38. Lente MH, Guerra JDS, de Souza GKS, Frygola BM, Raigoza CFV, Garcia D, Eiras JA (2008) Nature of magnetoelectric coupling in multiferroic $Pb(Fe_{1/2}Nb_{1/2})O_3$ ceramics. Phys Rev B 78:054109-1–054109-6
39. Correa M, Kumar A, Priya S, Katiyar RS, Scott JF (2011) Phonon anomalies and phono-spin coupling in oriented $Pb(Fe_{0.5}Nb_{0.5})O_3$ thin films. Phys Rev B 83:014302-1–014302-10
40. Katsura H, Nagaosa N, Balatsky AV (2005) Spin current and magnetoelectric effect in noncollinear magnets. Phys Rev Lett 95:057205-1–057205-4
41. Nugroho AA, Bellido N, Adem U, Nénert G, Simon C, Tjia MO, Mostovoy M, Palstra TTM (2007) Enhancing the magnetoelectric coupling in $YMnO_3$ by Ga doping. Phys Rev B 75:174435-1–174435-5
42. Lorenz B, Litvinchuk AP, Gospodinov MM, Chu CW (2004) Field-induced reentrant novel phase and a ferroelectric-magnetic order coupling in $HoMnO_3$. Phys Rev Lett 92:087204-1–087204-4
43. Singh A, Pandey V, Kotnal RK, Pandey D (2008) Direct evidence for multiferroic magnetoelectric coupling in $0.9BiFeO_3$–$0.1BaTiO_3$. Phys Rev Lett 101:247602-1–247602-4
44. Raevski IP, Prosandeev SA, Bogatin AS, Malitskaya MA, Jastrabik L (2003) High dielectric permittivity in $AFe_{1/2}B_{1/2}O_3$ nonferroelectric perovskite ceramics (A = Ba, Sr, Ca; B = Nb, Ta, Sb). J Appl Phys 93:4130
45. Raevski IP, Kuropatkina SA, Kubrin SP, Raevskaya SI, Titov VV, Sarychev DA, Malitskaya MA, Bogatin AS, Zakharchenko IN (2009) Dielectric and mössbauer studies of high-permittivity $BaFe_{1/2}Nb_{1/2}O_3$ ceramics with cubic and monoclinic perovskite structures. Ferroelectrics 379(1):48–54
46. Glazer AM (1972) The classification of tilted octahedral in perovskites. Acta Crystallogr B 28:3384–3392
47. Patel JP, Senyshyn A, Fuess H, Pandey D (2013) Evidence for weak ferromagnetism, isostructural phase transition, and linear magnetoelectric coupling in the multiferroic $Bi_{0.8}Pb_{0.2}Fe_{0.9}Nb_{0.1}O_3$ solid solution. Phys Rev B 88:104108-1–104108-9
48. Lee S, Pirogov A, Han JH, Park J-G, Hoshikawa A, Kamiyama T (2005) Direct observation of a coupling between spin, lattice and electric dipole moment in multiferroic $YMnO_3$. Phys Rev B 71:180413-1–180413-4

49. Raevski IP, Kubrin SP, Raevskaya SI, Sarychev DA, Prosandeev SA, Malitskaya MA (2012) Magnetic properties of $PbFe_{1/2}Nb_{1/2}O_3$: mossbauer spectroscopy and first-principles calculations. Phys Rev B 85:224412
50. Sitalo EI, Raevski IP, Lutokhin AG, Blazhevich AV, Kubrin SP, Raevskaya SI, Zakharov YN, Malitskaya MA, Titov VV, Zakharchenko IN (2011) Dielectric and piezoelectric properties of PbFe1/2Nb1/2O3-PbTiO3 ceramics from the morphotropic phase boundary compositional range. IEEE Trans Ultrason Ferroelectr Freq Control 58(9):1914–1919
51. Megaw HD, Darlington CNW (1975) Geometrical and structural relations in the rhombohedral perovskites. Acta Cryst A31:161–173